Applied Catalysis B: Environmental 89 (2009) 425–431

Contents lists available at ScienceDirect

Applied Catalysis B: Environmental

journal homepage: www.elsevier.com/locate/apcatb

Photoelectric catalytic degradation of methylene blue by C_{60}-modified TiO_2 nanotube array

Jie Lin, Ruilong Zong, Mi Zhou, Yongfa Zhu *

Department of Chemistry, Tsinghua University, Beijing, 100084, PR China

ARTICLE INFO

Article history:
Received 2 September 2008
Received in revised form 20 December 2008
Accepted 30 December 2008
Available online 15 January 2009

Keywords:
Photoelectrical catalysis
Fullerene
TiO_2 nanotube array
Methylene blue

ABSTRACT

Fullerene (C_{60})-modified TiO_2 nanotube array (TNA) was prepared by the electrophoresis deposition technique. The as-prepared samples showed the high efficiency for the photoelectric catalytic (PEC) degradation of nonbiodegradable azodyes methylene blue (MB). The highest PEC activity of C_{60}-modified TNA (TNA/C_{60}) was achieved at a lower bias potential (4.0 V), which was 2.3 times of the highest activity of TNA at 5.0 V. The high PEC activity came from the synergetic effect between C_{60} and TiO_2, which promoted the charge separation, influenced the charge distribution of the electrical double layer and reduced the impedances of the Helemholtz and depletion layers. Moreover, the oxidation of MB was a quick process during the PEC degradation, and the process began with the oxidation of the dimethylamino group, which was different from the photocatalytic (PC) process began with the oxidation of S atom; MB was mineralized completely during PEC degradation.

1. Introduction

Photocatalytic processes are a promising class of advanced oxidation technologies used for environmental remediation [1,2]. Among the photocatalysts, TiO_2 has been intensively investigated for the complete degradation of recalcitrant organic pollutants [2–4], because it is easily available, nontoxic, low-cost and chemically stable. However, TiO_2 has two typical shortcomings to render its wide application in practice: the difficult separation of TiO_2 from aqueous phase and relatively low quantum yield due to the rapid recombination of charge carriers. Now, the separation of photocatalyst from the solution suspension can be fulfilled by the immobilization of TiO_2 particles. Immobilization of TiO_2 on the supporter, especially on the conducting substrate, not only can eliminate the need for separation of photocatalyst from the solution suspension, but also can provide more advantages, such as using electrochemical technique to study and cooperate with photocatalytic process expediently [5,6]. For the advanced oxidation application, TNA has been considered as the most suitable way to achieve larger enhancement of surface area without an increase in the geometric area [7]. Among the fabrication methods of TNA, the electrochemical synthesis method shows its advantages of good mechanical adhesion strength and electronic conductivity since it directly grows from the titanium metal substrate [8]. In addition, the thickness and morphology of such TiO_2 film are easily controlled.

The high degree of recombination between photogenerated electrons and holes in semiconductor particles is a major limiting factor for photodegradation process [9]. Among the ways to enhance the separation of photogenerated charge carriers, the application of a low bias is an effective method. The bias drives the photogenerated electron to counter electrode in the PEC process, which could counteract the charge recombination process [10–12].

C_{60} have attracted extensive attentions for their various interesting properties due to their delocalized conjugated structures and electron-accepting ability. One of the most remarkable properties of C_{60} in electron-transfer processes is that it can efficiently arouse a rapid photoinduced charge separation and a relatively slow charge recombination [13]. Thus, the combination of photocatalysts and C_{60} may provide an ideal system to achieve an enhanced charge separation by photoinduced electron transfer. Some of the fullerene-donor linked molecules on an electrode exhibited excellent photovoltaic effects upon photo-irradiation [14–16]. Our previous study showed that the photocatalytic activities of Bi_2WO_6 were improved remarkably after C_{60} modification [17], the combination of C_{60} and TNA may be an ideal system for the PEC degradation of organic pollutant.

In this work, the enhanced PEC activity of TNA/C_{60} was reported. A series of experiments aimed to investigate the relationship between the C_{60} modification and the PEC activity

* Corresponding author. Tel.: +86 10 62783586; fax: +86 10 62787601.
E-mail address: zhuyf@tsinghua.edu.cn (Y. Zhu).

0926-3373/$ – see front matter © 2009 Published by Elsevier B.V.
doi:10.1016/j.apcatb.2008.12.025

were described. It showed that the enhanced activity was due to the synergistic effect of C_{60} and TNA. Moreover, the intermediates detected during the PEC process showed a different degradation path of MB from the PC process.

2. Experimental

2.1. Materials and preparation

All chemicals were analytical grade reagents and used without further treatment. Electrolyte was freshly prepared from deionized water. After chemical polishing, titanium foil (thickness about 250 μm, purity 99.4%, Beijing Cuibolin Non-Ferrous Technology Developing Co., Ltd.) was subjected to potentiostatic anodization in an electrochemical anodization cell with a platinum cathode in a 0.5 wt% HF + 1 M H_3PO_4 electrolyte at ambient temperature. The potential of 20 V was applied for 30 min. Then the samples were rinsed with deionized water and annealed at 450 °C for 24 h.

The TNA/C_{60} samples were prepared using electrodeposition method as in Ref. [18]. The electrolytic suspension was prepared by adding C_{60} (purity 99.9%, Peking University, PR China) to a mixture of acetonitrile and toluene (3:1, v/v). The electrodeposition was carried out potentiostatically using a CHI660B electrochemical system (Shanghai, China), with the TNA film as working electrode, a platinum wire as counter electrode and a standard calomel electrode (SCE) as reference electrode, respectively. The coverage of C_{60} on the TNA film was estimated by the charge passed (after the correction for solvent blank) during the electrodeposition.

2.2. Characterization

The structures of the TNA and TNA/C_{60} samples were characterized by XRD (Rigaku D/MAX-2500 X-ray powder diffractometer), using graphite monochromatized Cu Kα radiation (λ = 0.154 nm). A 0.02 step in 2θ/count, beam voltage of 40 kV and beam current of 300 mA were used. The phase composition of the samples was determined by Microscopic Confocal Raman Spectrometer (Renishaw, RM2000) using 632.8 nm as the exciting light source. Spectra were collected in the range of 1000–200 cm^{-1} with a resolution of 1 cm^{-1}. The morphologies and microstructures of the as-prepared samples were observed using a field emission scanning electron microscope (FE-SEM, LEO-1530) at 10 kV and a Tecnai TF20 high-resolution transmission electron microscope (HRTEM) operated at an accelerating voltage of 200 kV. Chemical characterization of the sample surface was recorded with scanning X-ray photoelectron spectroscopy (XPS, ULVAC-PHI, Quantera). The beam voltage was 3.0 kV, and the energy of Ar ion beam was 1.0 keV. The sputtering rate was approximately 9.5 nm/min for a thermally oxidized SiO_2 thin film. The binding energies were normalized to the signal for adventitious carbon at 284.8 eV.

2.3. Photoelectric properties and photoelectrocatalytic activities

All electrochemical and photoelectric studies were performed on a CHI660B electrochemical system (Shanghai, China) using a standard three-electrode cell with a working electrode (20 mm × 45 mm), a platinum wire counter electrode, and a SCE reference electrode. Photoelectrochemical properties were measured with an 18 W germicidal lamp (λ = 254 nm, Institute of Electric Light Source, Beijing). Unless otherwise stated, the intensity of light at the film electrode was 1.64 mW/cm^2 at the wavelength of 254 nm, and 0.1 M Na_2SO_4 electrolyte was used. The photocurrents were measured in the potential range of −0.3 to 1.0 V. The electrochemical impedance spectroscopies (EIS) were carried out at the open circuit potential. A sinusoidal ac perturbation of 5 mV was applied to the electrode over the frequency range of 0.05–10^5 Hz. The EIS spectra were further fitted and interpreted by Zsimpwin software. The catalytic activities of the samples were all evaluated by the removal of MB dye (with an initial concentration of 10 mg/L). The changes of MB concentration were monitored by the variations in absorption intensity at 660 nm using a UV–vis spectrometer (Hitachi U-3010). The mineralization of the dye was followed by measuring the total organic carbon (TOC) concentration, utilizing a Shimadzu Corporation TOC-V wp Analyzer.

2.4. Analyses of MB intermediates

To analyze the PEC process of MB, the original concentration of MB was increased to 50 mg/L, and the neutral products were enriched by 140 times. Before the analysis, the samples were filtered through millipore discs of 0.45 μm to protect the chromatographic column. HPLC monitoring was carried out using a UV absorbance detector (K 2501) operated at 280 nm coupled to a Venusil XBP-C18 (Agela Technologies Inc.) column. According to the literature [19], the reversed-phase eluent of pH 3 buffer and methanol (45:55, v/v) were used for aqueous solution, and water and methanol (40:60, v/v) was used for enriched neutral products. The neutral intermediates were finally identified by LC/MS (Thermo Fisher, LTQ).

3. Results and discussion

3.1. Photoelectric properties

The photoelectric properties of the TNA and TNA/C_{60} samples were evaluated by the photocurrent at bias 0 V and 1 V (Fig. 1). The amount of C_{60} on the TiO_2 film was expressed by the charge passing during the electrodeposition. It can be seen that the photocurrent was enhanced with the deposition charge and reached the maximum at 0.123 mC. The further increase decreased the photocurrent and finally reached its balance even the deposition charge increased to 0.41 mC. The highest photocurrent of TNA/C_{60} was 30% higher at 0 V and 40% higher at 1 V than that of TNA, respectively.

To investigate the influence of C_{60} modification on the photoelectric property, the EIS technology was used to study the solid/electrolyte interfaces of the TNA and TNA/C_{60} samples. According to conventional double-layer theories, the electrical double layer at the solid electrode behaved as a frequency distribution impedance instead of a pure capacitance due to the surface heterogeneity. When the charge transfer reaction occurred,

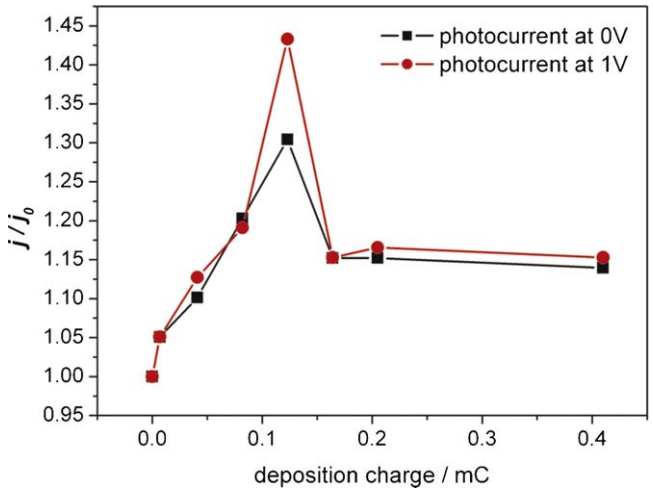

Fig. 1. Influence of deposition charge of C_{60} on the photoresponse for the TNA/C_{60} film.

the Nyquist plot was a semicircle; when semi-infinite diffusion was the rate-determining step, a linear with a slope of 45° appeared [20]. In our cases (Fig. 2a and b), only one semicircle on the EIS plane suggested charge transfer occurring, and the equivalent circuits were shown in Fig. 2c and d [21]: R_1, solution resistance; R_2, electric charge transfer resistance, corresponding to the Helmholtz layer; R_3, corresponding to the depleting layer; Q, the constant phase elements (CPE) of the inner layer of the TNA/C_{60} sample. Using the equivalent circuit, the impedance fitting values were shown in Fig. 2e and f. The electric charge transfer resistance (R_2) and the depleting layer resistance (R_3) under dark field decreased significantly with C_{60} modification and reached the balance when deposition charge of C_{60} increased to 0.082 mC.

The C_{60} on the surface increased the process of charge separation, influenced the distribution of the electrical double layer, and promoted the electron transfer, so that the electric charge transfer resistance (R_2) decreased. The charge distribution of electrical double layer also impacted the depleting layer, so that R_3 also decreased. With the increasing coverage of C_{60} on the surface of TNA film, the process of charge transfer reached the balance, and R_2 and R_3 were also invariable.

Under UV irradiation, the formation of photoinduced electron–hole pair reduced the resistance of depleting layer (R_3) by one order. Different from dark field, the Helmholtz layer was mainly occupied by the photoinduced electron–hole pair, so R_2 was also reduced by on order. The electron-transfer characterization of C_{60}

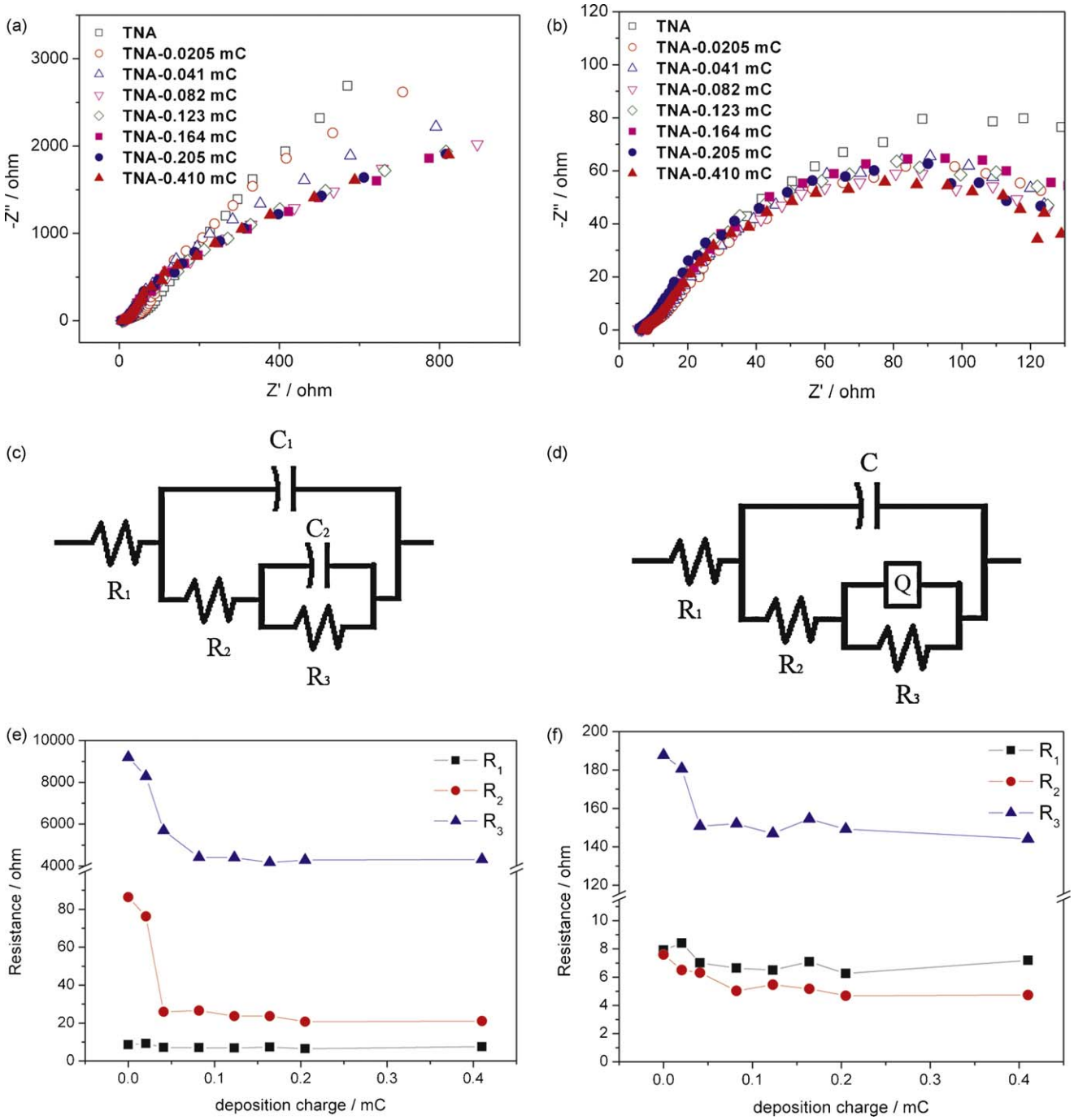

Fig. 2. Impedance spectra of TNA and TNA/C_{60} films (a) under dark and (b) under UV irradiation. Equivalent circuit supposed of TNA and TNA/C_{60} films (c) under dark and (d) under UV irradiation. Impedance fitting values of the TNA/C_{60} samples with different disposition charges (e) under dark and (f) under UV irradiation.

increased the charge separation process of the Helmholtz layer and changed the charge distribution of depleting layer availably. The smaller arc radius on EIS Nynquist plot of TNA/C_{60} film under UV irradiation meant an effective separation of photogenerated electron–hole pairs and fast interfacial charge transfer occurred [17]. On the other hand, the C_{60} on the TNA surface reduced the UV absorption and the contacting area between the TiO_2 and solution, which decreased the utilization efficiency of light. The enhanced charge separation process and reduced efficiency of light competed in our system, which caused the photoelectric properties increased initially then decreased to the balance, and the highest photo-response was obtained at the deposition charge of 0.123 mC.

3.2. Photoelectrocatalytic activities

The PEC activities of TNA and TNA/C_{60} (deposition charge of 0.123 mC) were evaluated by the degradation of MB under UV irradiation. Only 1% of MB was adsorbed on the TNA/C_{60} film after 2 h, so that the adsorption was not the main factor on the PEC process. According to the pseudo-first-order kinetic, the kinetic constants with the different biases were shown in Fig. 3a. As the electric catalytic (EC) degradation did not obey the pseudo-first-order kinetic, the percent of color removal after 90 min reaction was also given in Fig. 3b. It was seen that 12% of MB was removed at 6.0 V by EC process and 18.4% of MB was removed only under UV

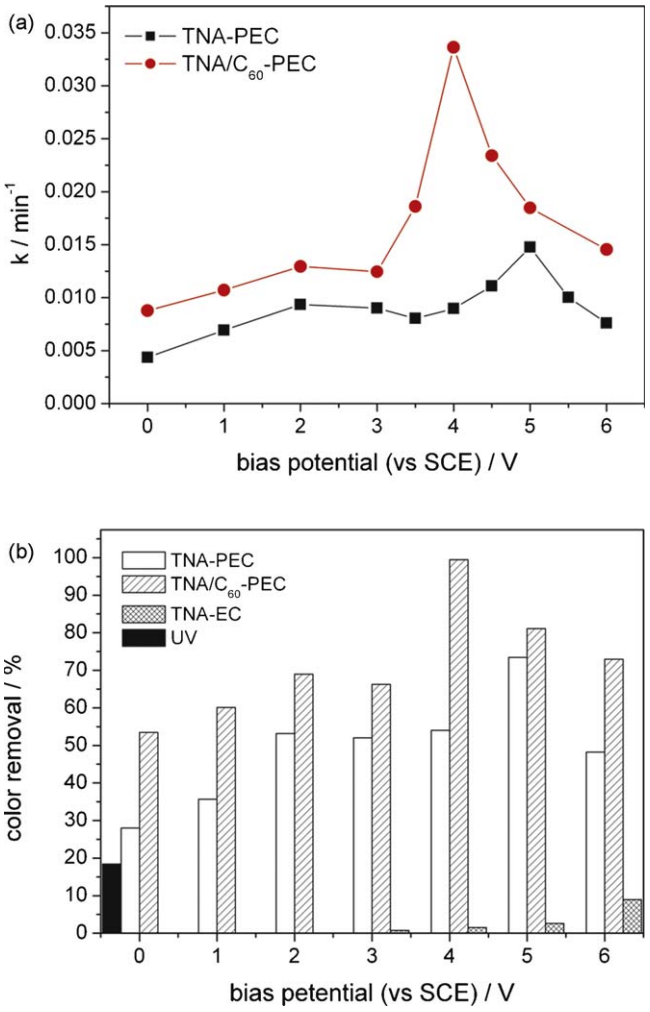

Fig. 3. The catalytic activity of TNA and TNA/C_{60} samples. (a) The pseudo-first-order kinetic constants of the PEC degradation of MB with TNA and TNA/C_{60} samples; (b) the color removal of MB within 1.5 h under PEC, EC, UV reaction, respectively.

irradiation, so that the EC process and UV irradiation were not effective routes to degrade MB. During the PEC process, the reaction rate increased initially then decreased with the increase of bias, which was similar to our previous study [22]. The low electrical bias between the anode and cathode, driving the photogenerated electron to counter electrode, could counteract the charge recombination process and improve the activity of TiO_2 [10,11]. The curve of cyclic voltammetry showed direct electric oxidation of MB on the TNA/C_{60} sample occurred above 3.2 V, and the oxygen evolution reaction occurred above 3.7 V (Support Information Figure S1). With the bias in the range of 2–3 V, the influence of bias on the separation of photoinduced electron–hole pair reached the balance, and the PEC activity could be attributed to the absolute amount of photoinduced electron–hole pair, which was constant under the UV irradiation of the same intensity. When the bias reached 3.2 V, the photoinduced-hole oxidation and the direct electro-oxidation of MB occurred together, and the photodegradation and electrochemical polymerization of MB competed on the sample surface. When the potential exceeded 3.7 V, the more active species such as hydroxyl radicals, H_2O_2, or O_3 could be produced [22], which lead to the indirect oxidation of MB. The mutual control of the three sides determined the maximum degradation rate reached at 4.0 V. With the bias further increasing, the process of electrochemical polymerization exceeded that of hole-oxidation and hydroxyl radicals' indirect oxidation, the polymer accumulated on the surface prevented the current conduction and decreased the degradation rate.

The presence of C_{60} reduced the resistance of Helmholtz layer and depleting layer, so the direct electro-oxidation and indirect oxidation of MB occurred at a lower bias. The presence of C_{60} also improved the separation of photoinduced electron–hole pairs and electron transfer, causing the increase of the photoelectrical activity. In a word, the modification of C_{60} on the surface enhanced the PEC activity of TNA and the highest activity can be achieved at a lower bias (4.0 V). As all the experiments were repeated, TNA/C_{60} was stable during the PEC process.

3.3. Intermediates during the PEC degradation of MB

To investigate the PEC process of MB, the composition of MB intermediates were detected by HPLC (Fig. 4). There were only two peaks separated from the chromatogram spectra of the original reaction solution. The previous study [19] indicated that two forms of MB existed in the solution (Support Information Scheme S2), so the two peaks at 4.5 and 4.6 min assigned to compounds II and I, respectively. It was clear that the compound II was degraded more quickly than the compound I during the PEC process, which suggested the compound II was more easily oxidized. To examine the process in detail, the neutral intermediates enriched by 140 times were also detected by HPLC (Fig. 4b) and further identified by LC/MS. The suggested structures of the intermediates based on the LC/MS results were shown in Table 1.

The neutral intermediates separated at 11.2, 11.6 and 17.7 min accumulated during the PEC process (Fig. 4b). The fact that all the three intermediates had a cyclohexa-2, 5-dienone structure suggested that the PEC process started with the oxidation of the dimethylamino group. Thus the compound II was considered as the initial reactant oxidized on the TiO_2 surface, so that the concentration of the compound II decreased more quickly. The minor intermediates separated at 8.0 and 8.5 min showed the primal oxidation at S atom, which was also observed at the initial step of MB degradation during the PC process [23]. These two intermediates suggested that a part of MB was degraded via the PC route. For the concentrations of all the neutral intermediates were low and the small molecules at 3.7 min did not accumulated markedly, it made evident that the PEC degradation was a quick

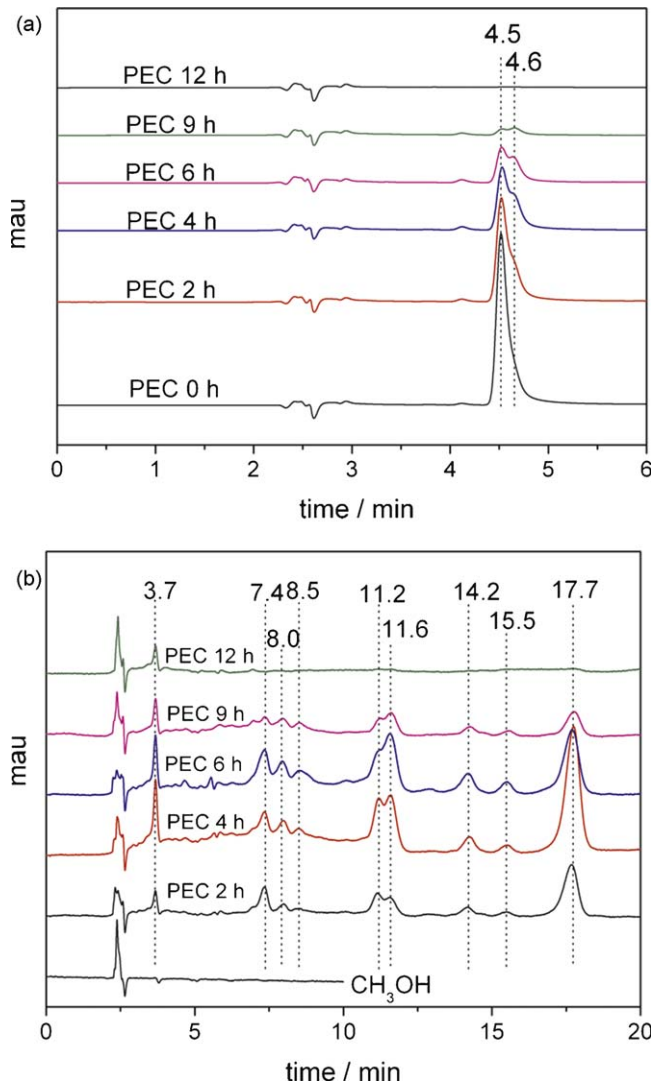

Fig. 4. Chromatograms of MB degradation products with the initial concentration of 50 ppm in photoelectrical system. (a) Original solution in methanol–buffer (55:45, v/v) eluent; (b) the neutral intermediates enriched by 140 times in methanol–water (60:40, v/v) eluent.

process. The mineralization of dye was also studied by measuring TOC removal. The samples corresponding to the HPLC results at 0 h and 12 h were used. After PEC process for 12 h, the TOC concentration decreased from 22.25 ppm to 4.37 ppm, namely 80% of TOC was removed by PEC oxidation. This result was consistent with the HPLC result. In a word, the photoelectrical oxidation of MB was a quick process and mainly began with the oxidation of the dimethylamino group; MB was mineralized by 80% during PEC degradation for 12 h.

3.4. Structure of TNA/C_{60} film

The XRD results (Support Information Figure S3) demonstrated that TiO_2 nanotube held the anatase phase before and after C_{60} modification. No diffraction peak of C_{60} was detected and C_{60} maybe existed in microcrystal or amorphous form. In addition, TiO_2 nanotube was oriented along [0 0 1] direction. The morphologies of the TNA and TNA/C_{60} were obtained by FESEM (Fig. 5a and b). The TNA was estimated 400 nm long, and the internal diameter was in the range of 50–70 nm. The morphology of TNA/C_{60} remained the same as that of TNA, and no aggregation of C_{60} was observed on the surface of the TNA/C_{60} sample. Further study by

Table 1
Suggested structures for the intermediates based on LC–MS results.

Retention time, t_R (min)	Structural formula	Molecular weight
3.7	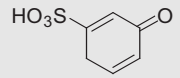	174
	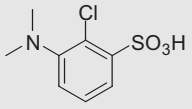	235
	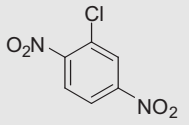	202
	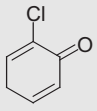	128
7.4	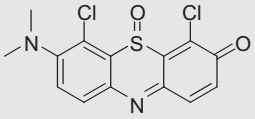	340
8.0	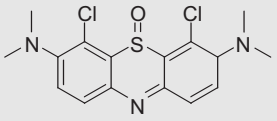	369
8.5	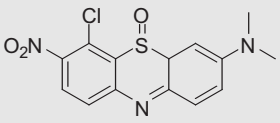	337
11.2	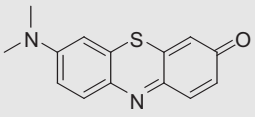	256
11.6	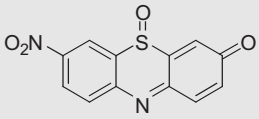	274
14.2	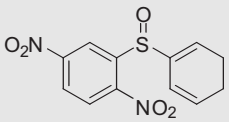	294
14.6	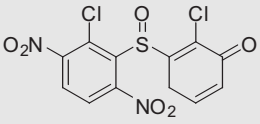	376
17.7	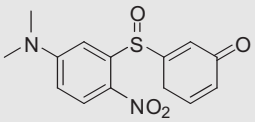	306

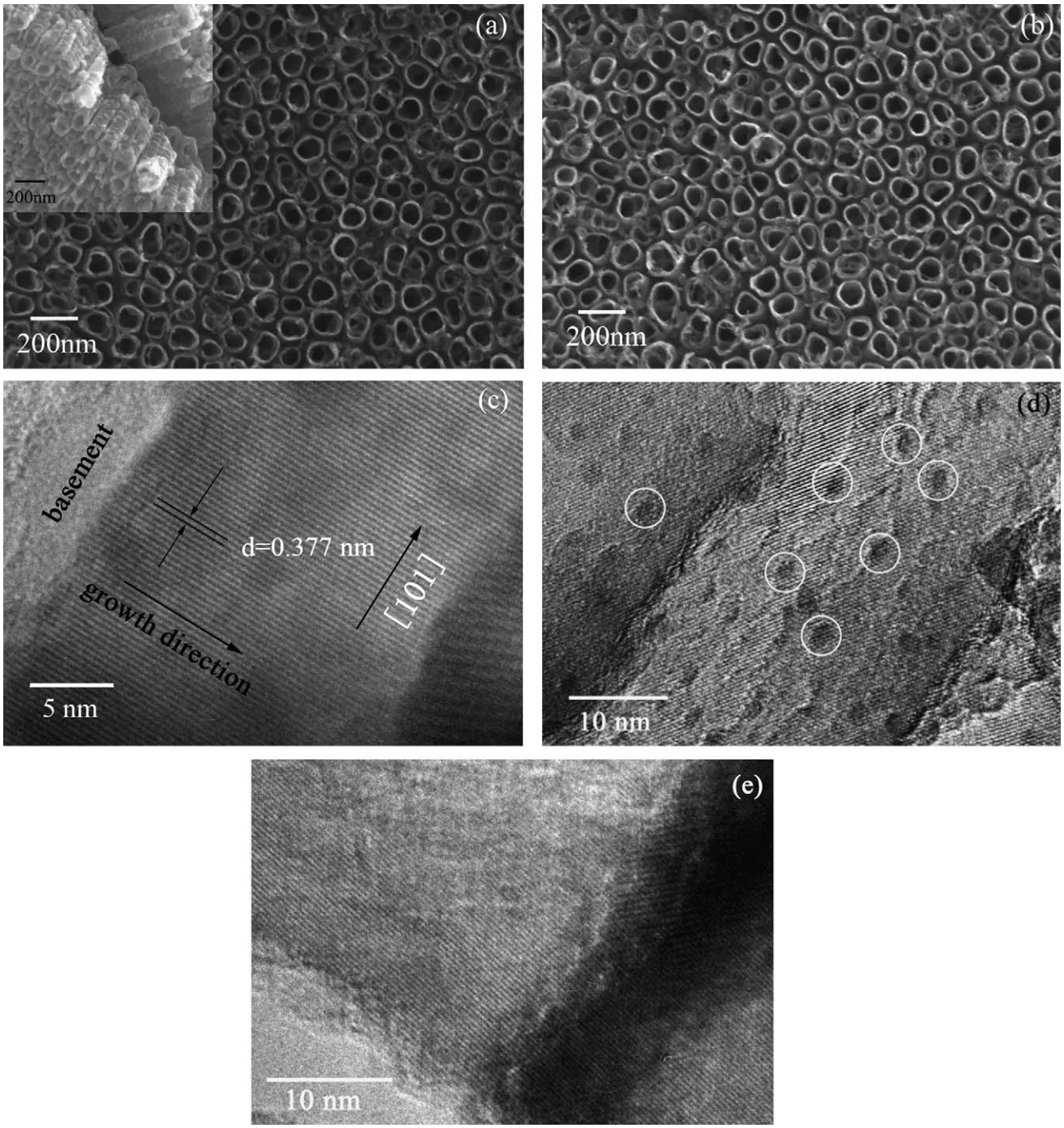

Fig. 5. Morphology of TNA and TNA/C_{60} samples: (a) FESEM image of TNA at the top view, the inset was that at the cross-section view; (b) FESEM image of TNA/C_{60} sample at the top view; (c) HRTEM image of the close-end of TNA/C_{60} sample lift-off from the film; (d) HRTEM image of the open-end of TNA/C_{60} sample with C_{60} clusters signed; (e) HRTEM image of the TNA sample.

HRTEM (Fig. 5c) showed the barrier layer (close-end) of TNA/C_{60} was structurally uniform with a lattice spacing of 0.377 nm corresponded to the (1 0 1) plane of anatase TiO_2 and the [1 0 0] direction was vertical to the growth direction. At the open-end of the TNA/C_{60} (Fig. 5d), some particles with amorphous form dispersed on the TiO_2 tube wall, and the average particle diameter was about 2 nm, which suggested that the C_{60} on the TiO_2 tube wall existed in the cluster form.

To confirm the existing form of C_{60} on the TiO_2 surface, the pristine C_{60}, TNA/C_{60} and fresh TNA samples were further characterized by Laser Raman spectroscopy (Fig. 6). The peaks of the TNA and TNA/C_{60} samples at 144, 397, 517 and 633 cm^{-1} belonged to the vibration mode of anatase phase, which confirmed the TiO_2 nanotube array held the anatase phase during the C_{60} modification. The two peaks of the pristine C_{60} at 1468 cm^{-1} and 1571 cm^{-1} were observed, which was corresponded to the Ag (2) and Hg (8) mode of C_{60} single crystal [24]. With Gaussian fitting, the wide peak of TNA/C_{60} around 1600 cm^{-1} was fitted to three peaks at 1561, 1580 and 1623 cm^{-1}, which connected with Hg (8) modes of C_{60}, the first-order G band and the disorder-induced D′ band of quasi-graphite structure, respectively [25]. Compared with the pristine C_{60}, the peaks of Ag (2) and Hg (8) modes in the TNA/C_{60} sample downshifted to 1460 and 1561 cm^{-1}, and the line widths increased observably. The downshift and increased line

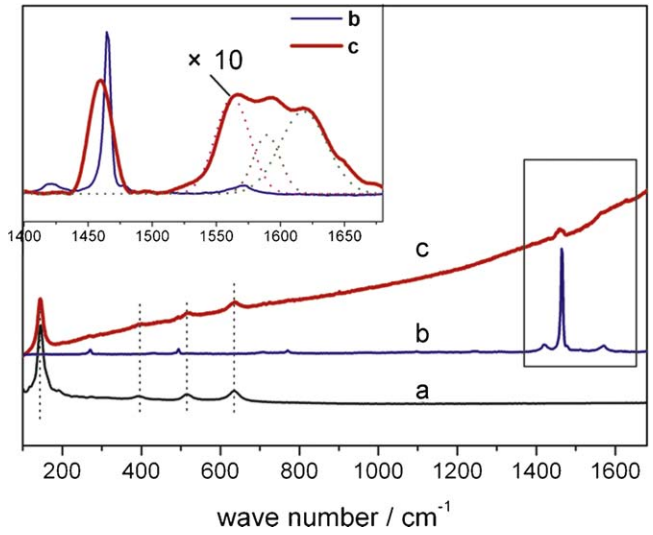

Fig. 6. Raman spectra for (a) TNA, (b) pristine C_{60} and (c) TNA/C_{60} samples. The inset was the comparison spectra of (b) and (c) in the range of 1400–1680 cm^{-1} after background correction.

widths of Ag pentagonal pinch mode indicated the electron transfer from TNA to C_{60} [26]. The appearance of G band and D′ band was supposed due to the partly ordered arrangement of C_{60} on the surface of TiO_2. The ordered arrangement of C_{60} increased the charge transfer and fluorescence by conjugation effect, so that Raman spectrum of the TNA/C_{60} sample displayed observable fluorescence background.

Based on the XPS results of TNA/C_{60} sample (Support Information Figure S4), the existence of the peak at 282.3 eV in C 1s spectrum and the peak at 457.6 eV in Ti 2p spectrum confirmed that C and Ti had a weak chemical interaction, which was consistent with the Raman results. Based on the results above, the coverage of the C_{60} on the TNA/C_{60} sample with the deposition charge of 0.123 mC was estimated in Supporting Information Figure S5. In the TNA/C_{60} sample of the best photoresponse (the deposition charge was 0.123 mC), nearly 88% of the TiO_2 tube wall was covered the C_{60} clusters.

4. Conclusions

In summary, TiO_2 nanotube array modified with C_{60} was formed by the electrodeposited method, and the synergetic effect between C_{60} and TNA enhanced charge separation process remarkably. C_{60} modification on the TNA surface with 88% coverage optimized the competition of enhanced charge separation process and reduced efficiency of light, and the sample obtained the highest photoelectric response. The enhanced charge separation process induced the TNA/C_{60} sample reached the highest PEC activity at a lower bias. Furthermore, the photoelectrical oxidation of MB was a quick process and began with the oxidation of the dimethylamino group on the TiO_2 surface; 80% of MB was mineralized during PEC degradation for 12 h.

Acknowledgements

This work was partly supported by Chinese National Science Foundation (20673065) and National Basic Research Program of China (2007CB613303).

Appendix A. Supplementary data

Supplementary data associated with this article can be found, in the online version, at doi:10.1016/j.apcatb.2008.12.025.

References

[1] M.R. Hoffmann, S.T. Martin, W. Choi, D.W. Bahnemann, Chem. Rev. 95 (1995) 69–96.
[2] A. Fujishima, T.N. Rao, D.A. Tryk, J. Photochem. Photobiol. C 1 (2000) 1–21.
[3] K.I. Hadjiivanov, D.K. Klissurski, Chem. Soc. Rev. 25 (1996) 61–69.
[4] A. Heller, Acc. Chem. Res. 28 (1995) 503–508.
[5] D.L. Jiang, S.Q. Zhang, H.J. Zhao, Environ. Sci. Technol 41 (2007) 303–308.
[6] W.X. Dai, X.X. Wang, P. Liu, Y.M. Xu, G.H. Li, X.Z. Fu, J. Phys. Chem. B 110 (2006) 13470–13476.
[7] Z.H. Zhang, Y. Yuan, G.Y. Shi, Y.J. Fang, L.H. Liang, H.C. Ding, L.T. Jin, Environ. Sci. Technol. 41 (2007) 6259–6263.
[8] Y. Xie, Electrochim. Acta 51 (2006) 3399–3406.
[9] A.L. Linsebigler, G. Lu, J.T. Yates Jr., Chem. Rev. 95 (1995) 735–758.
[10] K. Vinodgopal, S. Hotchandani, P.V. Kamat, J. Phys. Chem. 97 (1993) 9040–9044.
[11] K. Vinodgopal, P.V. Kamat, Sol. Energy Mater. Sol. Cells 38 (1995) 401–410.
[12] X. Quan, S. Yang, X. Ruan, H. Zhao, Environ. Sci. Technol. 39 (2005) 3770–3775.
[13] G. Yu, J. Gao, J.C. Hummelen, F. Wudl, A.J. Heeger, Science 270 (1995) 1789–1791.
[14] H. Hotta, S. Kang, T. Umeyama, Y. Matano, K. Yoshida, S. Isoda, H. Imahori, J. Phys. Chem. B 109 (2005) 5700–5706.
[15] D. Hirayama, T. Yamashiro, K. Takimiya, Y. Aso, T. Otsubo, H. Norieda, H. Imahori, Y. Sakata, Chem. Lett. (2000) 570–571.
[16] D.F. Liu, S.H. Yang, S.-T. Lee, J. Phys. Chem. C 112 (2008) 7110–7118.
[17] S.B. Zhu, T.G. Xu, H.B. Fu, J.C. Zhao, Y.F. Zhu, Environ. Sci. Technol. 41 (2007) 6234–6239.
[18] G.K.R. Senadeera, V.P.S. Perera, Chin. J. Phys. 43 (2005) 384–390.
[19] J.D. Donaldson, S.M. Grimes, N.G. Yasri, B. Wheals, J. Parrick, W.E. Errington, J. Chem. Technol. Biotechnol. 77 (2002) 756–760.
[20] J.Q. Li, L. Zheng, L.P. Li, Y.Z. Xian, L.T. Jin, J. Hazard. Mater. 139 (2007) 72–78.
[21] W.P. Gomes, D. Vanmaekelbergh, Electrochim. Acta 41 (1996) 967–973.
[22] X. Zhao, Y.F. Zhu, Environ. Sci. Technol. 41 (2006) 3367–3372.
[23] A. Houas, H. Lachheb, M. Ksibi, E. Elalour, C. Guillard, J.M. Herrmann, Appl. Catal. B: Environ. 31 (2001) 145–157.
[24] P. Bowmar, W. Hayes, M. Kurmoo, P.A. Pattenden, M.A. Green, P. Day, K. Kikuchi, J. Phys. Condens. Matter 6 (1994) 3161–3170.
[25] L.G. Cançado, A. Jorio, M.A. Pimenta, Phys. Rev. B 76 (2007) 064304.
[26] Y. Zhang, Y. Du, J.R. Shapley, M.J. Weaver, Chem. Phys. Lett. 205 (1993) 508–514.